2015

V2O5/mesoporous carbon composite as a cathode material for lithium-ion batteries

Mohammad Ihsan
University of Wollongong, mi314@uowmail.edu.au

Qing Meng
University of Wollongong, qm982@uowmail.edu.au

Li Li
University of Wollongong, li@uow.edu.au

Dan Li
Xinjiang University, Monash University, danli@uow.edu.au

Hongqiang Wang
University of Wollongong, hw571@uowmail.edu.au

See next page for additional authors

Publication Details

Ihsan, M., Meng, Q., Li, L., Li, D., Wang, H., Seng, K. Hau., Chen, Z., Kennedy, S. J., Guo, Z. & Liu, H. (2015). V_2O_5/mesoporous carbon composite as a cathode material for lithium-ion batteries. Electrochimica Acta, 173 172-177.

V2O5/mesoporous carbon composite as a cathode material for lithium-ion batteries

Abstract
V_2O_5/mesoporous carbon composite has been prepared by an ultrasonically assisted method followed by a sintering process. The as-prepared V_2O_5/mesoporous carbon material containing 90 wt% V_2O_5 shows better electrochemical performance, with capacity of 163 mA h g^{-1} after 100 cycles at the current density of 500 mA g^{-1}, as well as better charge/discharge rate capability for lithium storage than V_2O_5 nanoparticles. The improved electrochemical performance indicates that the V_2O_5/mesoporous carbon composite could be used as a promising cathode material for lithium ion batteries.

Keywords
ion, lithium, material, batteries, cathode, carbon, composite, mesoporous, v2o5

Disciplines
Engineering | Science and Technology Studies

Publication Details
Ihsan, M., Meng, Q., Li, L., Li, D., Wang, H., Seng, K. Hau., Chen, Z., Kennedy, S. J., Guo, Z. & Liu, H. (2015). V_2O_5/mesoporous carbon composite as a cathode material for lithium-ion batteries. Electrochimica Acta, 173 172-177.

Authors
Mohammad Ihsan, Qing Meng, Li Li, Dan Li, Hongqiang Wang, Kuok Hau Seng, Zhixin Chen, Shane J. Kennedy, Zaiping Guo, and Hua-Kun Liu

V_2O_5/Mesoporous Carbon Composite as a Cathode Material for Lithium-ion Batteries

Mohammad Ihsan [a,b], Qing Meng[a], Li Li[a], Dan Li[a], Hongqiang Wang[a], Kuok Hau Seng[a], Zhixin Chen[c], Shane J. Kennedy[d], Zaiping Guo**[a,c], and Hua-Kun Liu*[a]

[a] *Institute for Superconducting and Electronic Materials, ARC Centre of Excellence for Electromaterials Science, University of Wollongong, NSW 2522, Australia*
[b] *PSTBM – BATAN, Kawasan PUSPIPTEK Serpong, Tangerang Selatan, Banten 15314 Indonesia*
[c] *School of Mechanical, Materials and Mechatronic Engineering, University of Wollongong, NSW 2500, Australia*
[d] *Bragg Institute, Australian Nuclear Science and Technology Organization, Lucas Heights, NSW 2234, Australia*
Corresponding author. **Tel:+61 2 4221 4547 **Fax:**+61 2 4221 5731. Email address: hua_liu@uow.edu.au; hua@uow.edu.au*
***Corresponding author. **Tel**:+61 2 4221 1490 **Fax:**+61 2 4221 5731. Email address: zguo@uow.edu.au*

ABSTRACT

V_2O_5/mesoporous carbon composite has been prepared by an ultrasonically assisted method followed by a sintering process. The as-prepared V_2O_5/mesoporous carbon material containing 90 wt% V_2O_5 shows better electrochemical performance, with capacity of 163 mA h g^{-1} after 100 cycles at the current density of 500 mA g^{-1}, as well as better charge/discharge rate capability for lithium storage than V_2O_5 nanoparticles. The improved electrochemical performance indicates that the V_2O_5/mesoporous carbon composite could be used as a promising cathode material for lithium ion batteries.

***Keywords**: vanadium pentoxide; mesoporous carbon; cathode; lithium ion batteries*

1. Introduction

Nowadays, rechargeable Li-ion batteries (LIBs) are extensively used in almost all types of

electronic devices, including cell phones, laptop computers, camcorders, and even electric and hybrid electric vehicles, due to their high energy and power density, high voltage, and long lifespan [1-3]. The worldwide market for lithium ion batteries is growing fast, especially for consumer products, and it will grow even more in the next decade. Frost & Sullivan, a business consulting firm, has reported that the global lithium-ion battery market in 2012 was worth $11.7 billion, mainly for consumer applications, and this is expected to be twice as great, around $22.5 billion, in 2016 [4].

Until now, $LiCoO_2$, which was first introduced by SONY, has been the most commonly used cathode material in LIBs. Due to the toxicity, high cost, and safety issues of $LiCoO_2$, however, many efforts have been made to develop other cathode materials, such as $LiNi_{1/3}Mn_{1/3}Co_{1/3}O_2$, $LiMn_2O_4$, and $LiFePO_4$ [5-7]. These materials have shown significant improvements in their cycling stability and rate capability. Enhancement of their reversible lithium storage capacity has been limited, however, due to their intrinsic redox chemistry, which allows only one Li^+ insertion/extraction per formula unit. Hence, new materials need to be developed as cathode candidates with enlarged theoretical capacity through multi-electron reactions per formula unit, in order to comply with the demand for LIBs with high capacity and fast charge capability.

Among the many potential cathode candidates, vanadium pentoxide (V_2O_5) is one of the most promising due to its high energy density, abundance, low cost, and easy to synthesize [8-12]. The high theoretical capacity of V_2O_5 is especially attractive, around 294 mA h g^{-1} for the intercalation/deintercalation of two Li^+ ions between 2.0 and 4.0 V, which is much better than those of conventional cathode materials, such as $LiMn_2O_4$ (148 mA h g^{-1}) and $LiFePO_4$ (176 mA h g^{-1}). In spite of these advantages, the electrochemical performance of V_2O_5 is limited by its poor electrical conductivity (10^{-3} to 10^{-2} S cm^{-1}) and its sluggish diffusion of lithium ions (~ 10^{-12} cm^2 s^{-1}) [13-16]. Moreover, phase transitions of $Li_xV_2O_5$ during the charge/discharge process often

cause structural instability and can further degrade its cycling performance [17-19]. These drawbacks have limited the practical application of this material in commercial LIBs. Several approaches have been tried to solve these issues: fabricating nanostructures, changing the pore size, and modifying the electrical conductivity with a carbon matrix [11-13, 15, 18, 20-45].

One approach to address these issues is modifying the V_2O_5 with ordered mesoporous carbon. Mesoporous carbon, which has pore sizes between 2 and 50 nm, will facilitate electrolyte diffusion into the bulk of the electrode material and hence provide fast transport channels for the conductive ions (i.e. Li^+ ions). Carbon will also provide fast electronic transport, which may enhance the overall performance of lithium ion batteries. The other properties of mesoporous carbon, such as its high thermal stability, large surface area, uniform pore diameter, high pore volume, and interconnected pore structure, also increase its potential value in lithium ion batteries [46, 47]. Some metal oxide/mesoporous carbon composites have already been synthesized, such as ones containing Sn/SnO_2, SnO_2, Cr_2O_3, and TiO_2, as electrode materials for lithium ion batteries [18-22]. V_2O_5-mesoporous carbon composite as an electrode material for capacitors has also been reported by Yu et al. [48]. In this work, we use mesoporous carbon to prepare V_2O_5-mesoporous carbon composite as a cathode material for LIBs. The mesoporous structure of the carbon helps the diffusion of electrolyte into the bulk of the electrode and, as a result, provides fast transport channels for Li^+ ions.

2. Experimental

Preparation of mesoporous carbon

The mesoporous carbon was synthesized in a similar way to the procedure reported by C. F. Xue et al. [49] with a slight modification. Firstly, a resol solution was prepared as the carbon precursor. Phenol (61 g) was melted at 42 ºC in a flask, and 20 mL 20 wt% NaOH solution was then slowly added under stirring over a period of 20 minutes. After that, 100 mL formalin (37

wt%) was added to the solution, and the mixture was heat-treated at 70 ºC for 1 h. The pH of the mixture was adjusted to 7.0 after cooling down to room temperature naturally. Water was then eliminated under vacuum at a temperature below 50 ºC, and the obtained product (resol solution) was dissolved in ethanol (40 wt%).

The mesoporous-carbon-silica composite monoliths were prepared via evaporation-induced coating self-assembly (EISA). In a typical synthesis, 16 g F127 triblock copolymer was dissolved in a mixture of ethanol (82 mL) and 0.2 M HCl (10 mL), and stirred for 1 h at 40 ºC. Then, the resol solution was slowly added to this solution under stirring for 10 min, followed by the addition of 20.8 g tetraethyl orthosilicate (TEOS), and stirring was continued for 2 h at ambient temperature. The obtained solution was poured onto polyurethane (PU) foam. The air bubbles inside the PU foam were eliminated by regularly squashing the foam with a glass rod during the infusion process. The infused PU foam was turned constantly for 5–8 h to vaporize the solvent. Then, the PU foam was heated at 100 ºC for 20 h in an oven for further thermopolymerization. The calcination was carried out at 900 ºC for 3 h under flowing N_2, with heating rates of 1 ºC min^{-1} below 600 ºC and 5 ºC min^{-1} above 600 ºC, so that a mesoporous composite was obtained. Then, the resultant composite was washed in boiled NaOH solution (2.5 M) to remove the silica in order to obtain mesoporous carbon. Surface modification of the mesoporous carbon was performed in the following way: 1 g mesoporous carbon was added into 100 mL HNO_3 (20 wt%) and stirred for 3 h at 80 ºC. The resultant product was recovered by filtration and washed with deionized water until the filtrate pH was 7. Then, the product was added into 100 g of H_2O_2 30 wt% solution and stirred at room temperature for 30 min, after which, the stirring was continued at 60 ^oC for 1 h. Finally, the product was obtained by filtration, washed thoroughly with water, and dried at 80 ^oC for 12 h.

Preparation of V_2O_5/mesoporous carbon

V_2O_5 was prepared by the sol method by stirring 0.5 g V_2O_5 powder into 50 mL H_2O_2 (30 wt%) for 24 h at room temperature [50]. Then, 0.2 g mesoporous carbon was dispersed into the V_2O_5 sol, and the mixture was stirred for 1 h. After that, the mixture was ultrasonicated for 3 h at room temperature. The precipitate was filtered and washed with distilled water and ethanol. Then, the solvent was removed by drying at 120 ºC for 12 h. The resultant product (denoted as V_2O_5/mc before sintering) was divided into three portions: the first portion was reserved without further treatment, another portion was sintered at 550 ºC in air atmosphere for 2 h with a 5 ºC min^{-1} heating rate to burn away the carbon to produce V_2O_5 nanoparticles (denoted as V_2O_5 np), and the third portion was sintered at 300 ^oC for 5 h in air atmosphere (denoted as V_2O_5/mc).

Characterisation

The specific surface area (determined by the Brunauer-Emmett-Teller (BET) method) and nitrogen adsorption-adsorption isotherms of samples of mesoporous carbon and V_2O_5/mc before sintering were measured in order to observe the effects of the insertion process on the properties of the mesoporous carbon. V_2O_5/mc before sintering was examined by transmission electron microscopy (TEM; JEOL 2010 and JEOL ARM-200F) in order to determine whether the insertion process of V_2O_5 into the mesoporous carbon was successful or not.

All the resultant products were characterised by X-ray diffraction (XRD; GBC MMA Diffractometer, Cu Kα radiation, λ = 1.5406 Å). The content of V_2O_5 in the V_2O_5/mc was investigated by thermogravimetric analysis (TGA; Mettler Toledo TGA/DSC1), which was taken into account in the battery testing. For electrochemical performance testing, working electrodes were prepared by mixing 85 wt% active material, 6 wt% conductive agent (carbon black, Super-P-Li), and 9 wt% polyvinylidene difluoride (PVDF) binder (Sigma-Aldrich) in N-methyl-2-pyrrolidinone (NMP) to form a homogeneous slurry. The slurry was uniformly pasted onto

aluminium foil and dried in a vacuum oven at 120 °C for 12 h. Electrochemical cells (CR2032 coin type) containing the working electrode and Li foil as the counter and reference electrode were assembled in an Ar-filled glove box (Mbraun, Unilab, USA). 1 M $LiPF_6$ in a 3:4:3 (v/v) mixture of ethylene carbonate (EC), dimethyl carbonate (DMC), and diethyl carbonate (DEC), with 5% fluoroethylene carbonate (FEC) additive was used as the electrolyte. The galvanostatic charge-discharge measurements were performed on a Land CT2001A battery tester.

3. Results and discussion

Fig. 1 presents the nitrogen adsorption–desorption isotherms and the pore size distribution curves of the mesoporous carbon (mc) and V_2O_5/mc composites before sintering. As can be seen in Figure 1(a), N_2 sorption isotherms of both samples show hysteresis and therefore represent type-IV behaviour, according to the IUPAC classification, indicating mesoporous structure. Fig. 1(b) reveals that the main pore size of the mesoporous carbon (mc) is about 3 nm, and the pore size decreases to 2-3 nm after insertion of V_2O_5. This is consistent with the BET surface area and total pore volume data for the mesoporous carbon and the V_2O_5/mc before sintering, as summarized in Table 1. The BET surface area (S_{BET}) of the V_2O_5/mc before sintering is decreased significantly compared to that of mesoporous carbon matrix alone, which are calculated to be 77.2 and 874 $m^2 g^{-1}$, respectively. This clearly indicates that the V_2O_5 nanoparticles have filled most of the pores in the mesoporous carbon. The total pore volumes of the mc and the V_2O_5/mc composite are 0.76 and 0.06 $cm^3 g^{-1}$, respectively which also demonstrates that the V_2O_5 nanoparticles block the pore channels.

The TEM images and energy dispersive spectroscopy (EDS) results confirm the dispersion of the V_2O_5 particles in the pores of the mesoporous carbon. Fig. 2(a) shows the highly ordered mesoporous carbon in the mesoporous carbon sample. Scanning transmission electron microscope

(STEM) images of V_2O_5/mc before sintering are presented in Fig. 2(b) and (c), which are in bright field (BF) and annular dark field (ADF) mapping mode, respectively. Amorphous structures of carbon and lattice fringes of V_2O_5 are observed in the BF mode figure. In the ADF mapping mode, the dark contrast is from the pores of carbon without any V_2O_5 particles, while the light contrast reflects the very fine particles of V_2O_5 in the occupied pores of mesoporous carbon. The EDS spectrum in Fig. 2(d) of the area in Fig. 2(b) and (c) confirms the presence of V_2O_5 in the sample.

We have applied two strategies to prevent the coating of V_2O_5 on the carbon. Firstly, the V_2O_5 was dissolved in H_2O_2 to form a V_2O_5 sol. Secondly, due to the capillary effect of the mesopores and the applied ultrasonication, the majority of V_2O_5 can be sucked into the pores of the mesoporous carbon. BET test results have confirmed the insertion of the V_2O_5 particles into the pores of the carbon. The TEM image in Figure 2(b) shows some light contrast representing pores in the carbon and some dark contrast representing V_2O_5 in the occupied pores, confirming that our strategies have been successful.

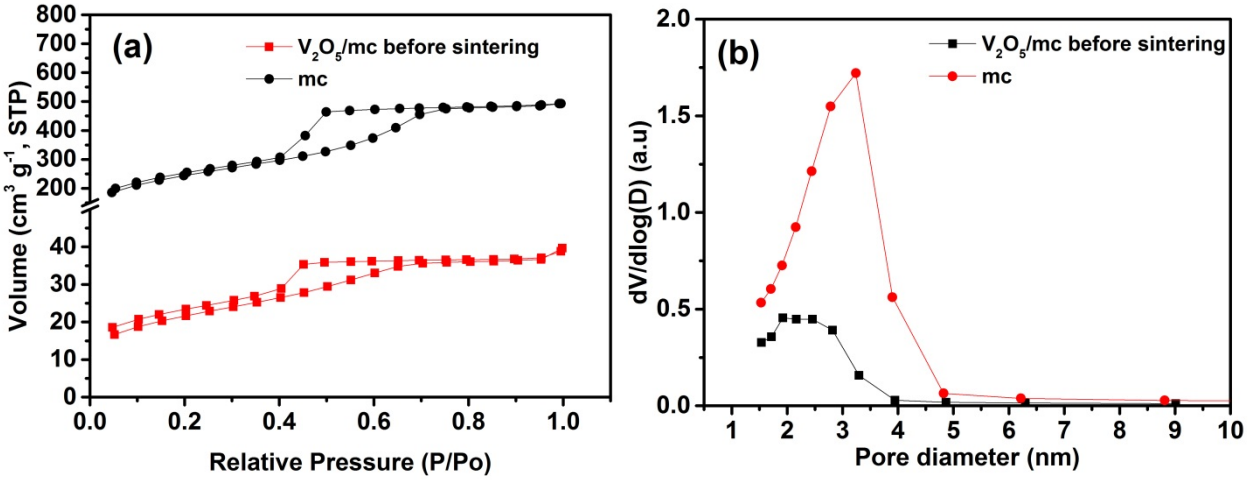

Figure 1. (a) Nitrogen adsorption-desorption isotherms; (b) pore size distributions of mesoporous carbon (mc) and V_2O_5/mc before sintering.

Table 1. BET surface area and total pore volume per gram of the mesoporous carbon and the V_2O_5/mc before sintering.

Sample	S_{BET} ($m^2 g^{-1}$)	V_{pore} ($cm^3 g^{-1}$)
Mesoporous carbon (mc)	874	0.76
V_2O_5/mc before sintering	77.2	0.06

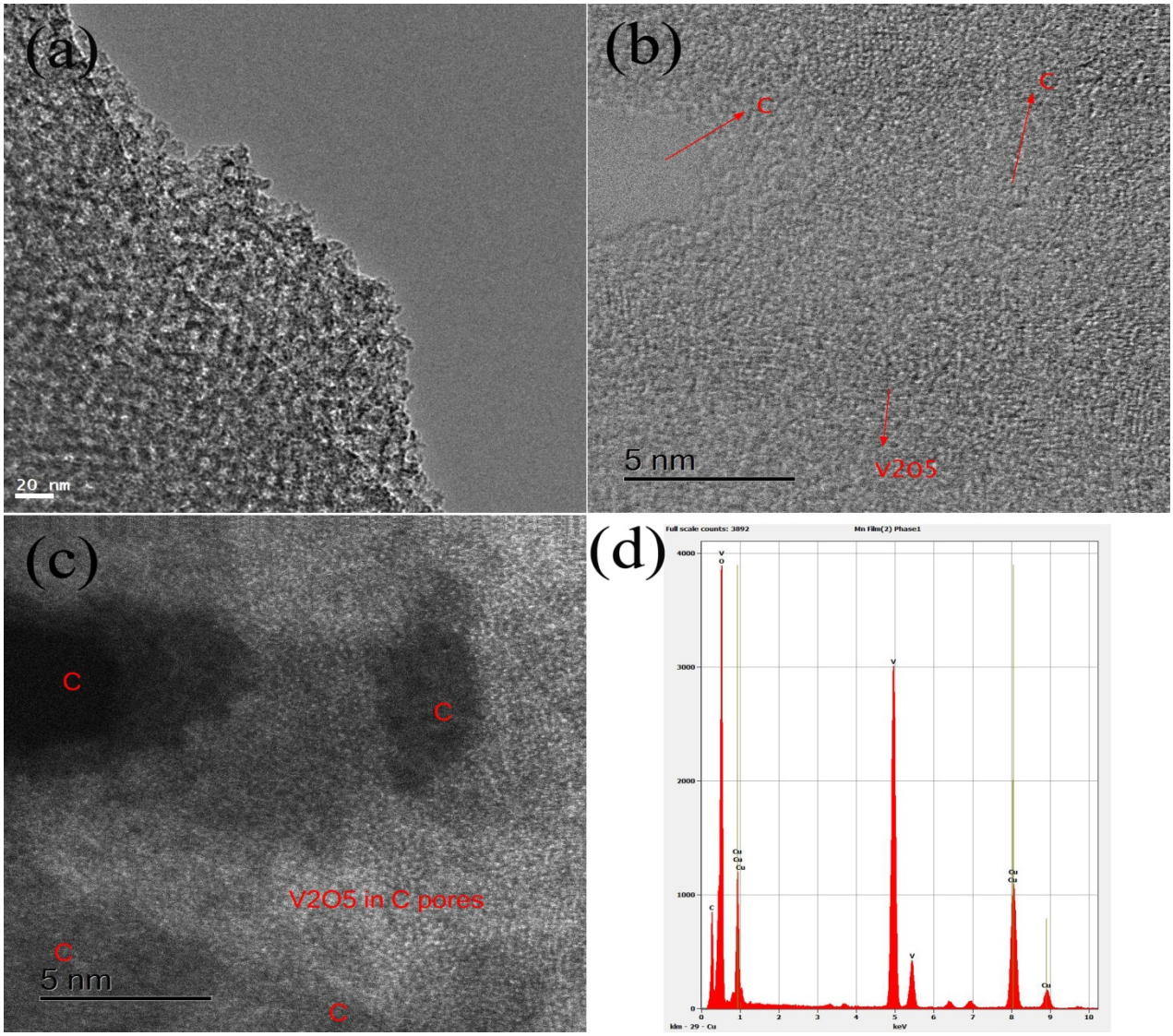

Figure 2. (a) TEM image of mesoporous carbon sample; (b) STEM image of V_2O_5/mc before sintering in BF mapping mode; (c) STEM image of V_2O_5/mc before sintering in ADF mapping mode (with dark contrast representing pores of carbon, light representing pores + V_2O_5 particles); (d) EDS spectrum of the area in (b) and (c) (with the Cu peak coming from the TEM sample holder).

The reactions of V_2O_5 powder and H_2O_2 in the order used to make V_2O_5 sol can be described by the following reactions [39]:

$$xV_2O_5 + 4xH_2O_2 + yH_2O \rightarrow 2x[VO(O_2)_2]^- + 2xH^+ + (3x + y)H_2O \quad \text{……(1)}$$

$$2x[VO(O_2)_2]^- + 2xH^+ + (3x + y)H_2O \rightarrow (2x - a)[VO(O_2)_2]^- + a[VO(O_2)]^+ + 2(x - a)H^+ + 0.5aO_2\uparrow + (3x + y + a)H_2O \quad \text{...……...(2)}$$

$$(2x - a)[VO(O_2)_2]^- + a[VO(O_2)]^+ + 2(x - a)H^+ + 0.5aO_2\uparrow + (3x + y + a)H_2O \rightarrow c[VO_2]^+ + (2x - c - 10b)[VO(O_2)]^+ + b[H_nV_{10}O_{28}]^{(6-n)-} + (x + 0.5c + 5b)O_2\uparrow + (4x + y - 0.5nb)H_2O \; [n = (16b - 2x)/b] \quad \text{……..……..….(3)}$$

$$c[VO_2]^+ + (2x - c - 10b)[VO(O_2)]^+ + b[H_nV_{10}O_{28}]^{(6-n)-} + (x + 0.5c + 5b)O_2\uparrow + (4x + y - 0.5nb)H_2O \; [n = (16b - 2x)/b] \rightarrow 2x - 10d)[VO_2]^+ + d[H_nV_{10}O_{28}]^{(6-n)-} + 2xO_2\uparrow + (4x + y - 0.5nd)H_2O[n = (16d - 2x)/d] \quad \text{……..……...…..(4)}$$

$$2x - 10d)[VO_2]^+ + d[H_nV_{10}O_{28}]^{(6-n)-} + 2xO_2\uparrow + (4x + y - 0.5nd)H_2O[n = (16d - 2x)/d] \rightarrow xV_2O_5 \cdot [4 + (y/x)]H_2O + 2xO_2\uparrow \quad \text{……...…….(5)}$$

$xV_2O_5 \cdot [4 + (y/x)]H_2O$ represents the resulting vanadium pentoxide sol. In lithium ion battery tests, the resulting vanadium pentoxide sol sample will suffer from poor electrochemical performance due to the crystal water, and therefore, a sintering process at 300 ^oC for 5 h was applied to the V_2O_5/mc before sintering sample to further remove the crystal water. Fig. 3 (a) presents the XRD patterns of V_2O_5/mc, V_2O_5 np, and V_2O_5/mc before sintering. The XRD patterns of V_2O_5/mc and V_2O_5 np indicate that all the diffraction peaks are in good agreement with the standard pattern of orthorhombic V_2O_5 (space group: Pmnm (No. 59), a = 1.1516 nm, b = 0.3565 nm, c = 0.4372 nm, JCPDS card No. 41-1426). In contrast, the pattern of V_2O_5/mc before sintering shows two diffraction peaks at 26.2º and 51.3º. The weakness and broadness of the peaks indicate the poor crystallization and small crystallite size of the vanadium pentoxide. It can be concluded that ultrasonic treatment inhibits the aggregation of vanadium pentoxide.

The content of V_2O_5 in the V_2O_5/mc sample (after sintering) was examined by thermogravimetric analysis (TGA) in air (Figure 3 (b)). As illustrated in the Figure, the weight loss before 150 ºC can be assigned to the evaporation and removal of moisture. When the heating

was continued to 550 ºC, the weight loss could be determined to be carbon removal. The content of V_2O_5 in the V_2O_5/mc sample after sintering is 90 wt%, which was taken into account in the battery testing.

The rate capabilities of V_2O_5/mc and V_2O_5 np were measured at various current densities between 2 and 4 V. Figure 4(a) presents the rate capability of V_2O_5/mc, which is better than that of V_2O_5 np. The V_2O_5/mc electrode displays better performance than the V_2O_5 np electrode at all current densities. The capacities of V_2O_5/mc are 291, 265, and 247 mA g^{-1}, at current densities of 100, 250, and 500 mA g^{-1}, respectively. In contrast, the capacity of V_2O_5 np rapidly decreases as the current density is increased. It shows the capacities of 275, 235, and 182 mA g^{-1} at current densities of 100, 250, and 500 mA g^{-1}, respectively. After a deep cycling at 5 A g^{-1}, the V_2O_5/mc electrode can almost recover its initial capacity when the current density is returned to 100 mA g^{-1}. Evidently, the V_2O_5/mc sample demonstrates higher capacity at every current density. The V_2O_5/mc electrode also shows improved rate capability performance compared with those of V_2O_5/rGO [40], V_2O_5/PEDOT/MnO_2 nanowire [41], multiwalled CNT- V_2O_5 [39], V_2O_5 nanosheet /RGO [42], and graphene nanoribbon / V_2O_5 [43], as shown in Table 2.

The cycling performances of V_2O_5/mc and V_2O_5 np samples at a current density of 500 mA g^{-1} are shown in Figure 4(b). The capacity retention of V_2O_5/mc is considerably higher than that of V_2O_5 np. A better reversible capacity of 163 mAh g^{-1} is maintained after 100 cycles, which represents a capacity loss of 40 %, while the capacity of V_2O_5 np electrode declines to around 50 % after 100 cycles. V_2O_5/mc with capacity of 198 mAh g^{-1} after 50 cycles also shows comparable or better performance in comparison with several V_2O_5/carbon composites from recently published works (Table 2), for example, V_2O_5/rGO (105 mAh g^{-1} at 5700 mA g^{-1}) [40], V_2O_5/PEDOT/MnO_2 nanowire (166 mAh g^{-1}after 40 cycles at 50 mA g^{-1}) [41], multiwalled CNT-V_2O_5 (199 mAh g^{-1} at 100 mA g^{-1}) [39], V_2O_5 nanosheet /RGO (150 mAh g^{-1} at 600 mA g^{-1}) [42], and graphene nanoribbon / V_2O_5 (230 mAhg^{-1} at 30 mA g^{-1}) [43].

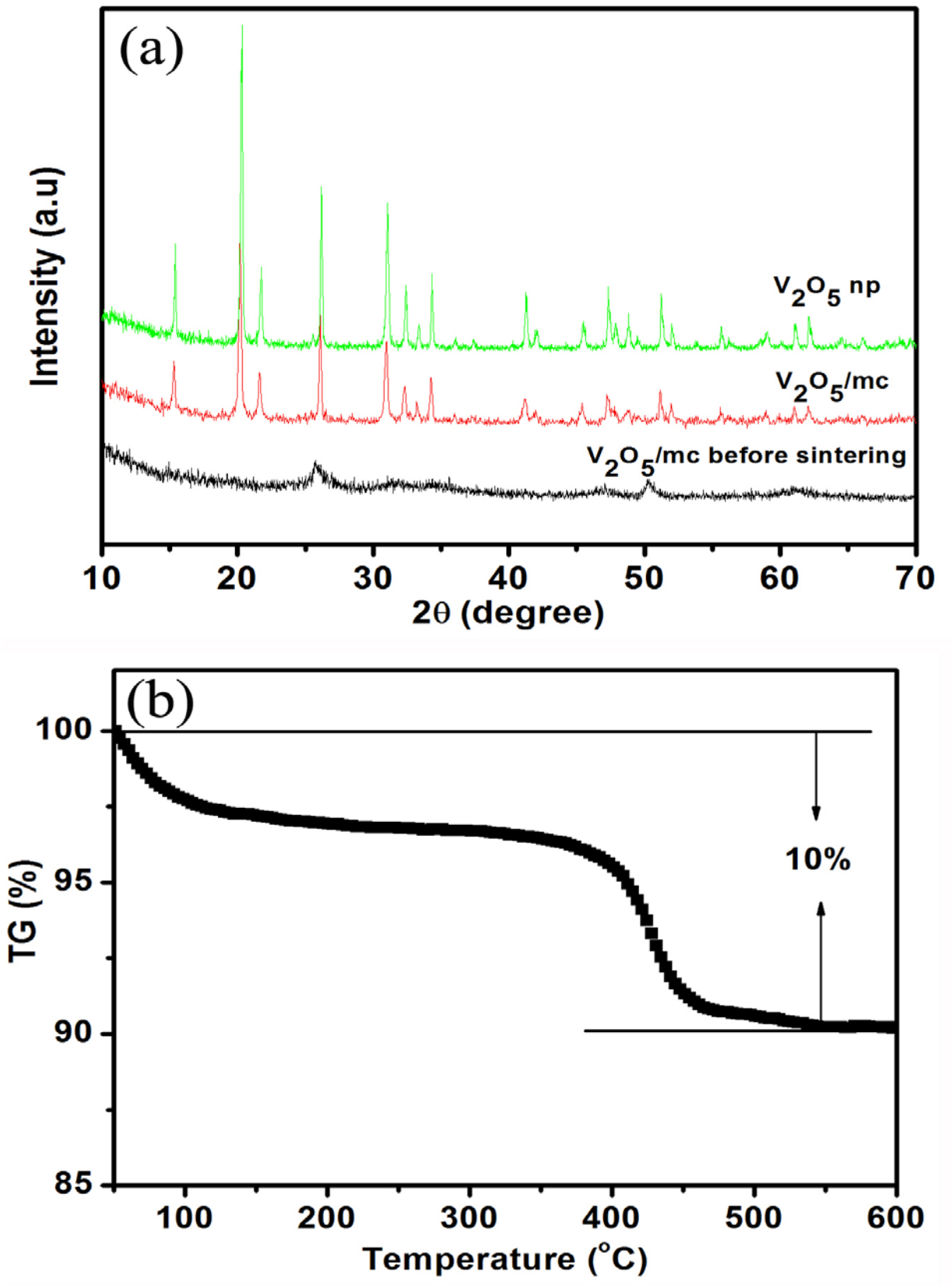

Figure 3. (a) XRD patterns of V_2O_5 nanoparticles (V_2O_5 np) and of V_2O_5/mesoporous carbon (V_2O_5/mc) before and after sintering; (b) TGA curve of V_2O_5/mesoporous carbon (V_2O_5/mc) after sintering

We have also synthesized a composite of V_2O_5 nanoparticles and mesoporous carbon made by simple mixing (denoted as V_2O_5/mc sm) for comparison. Its rate capability and cycling performance, as shown in Figure 4(a) and (b), are not as good as those of V_2O_5/mc produced by the ultrasonication technique. The lower rate capability and cycling performance indicate that the mesoporous structure plays an important role in Li^+ ion transport that the performance will be improved much more by the insertion of V_2O_5 particles into the pores.

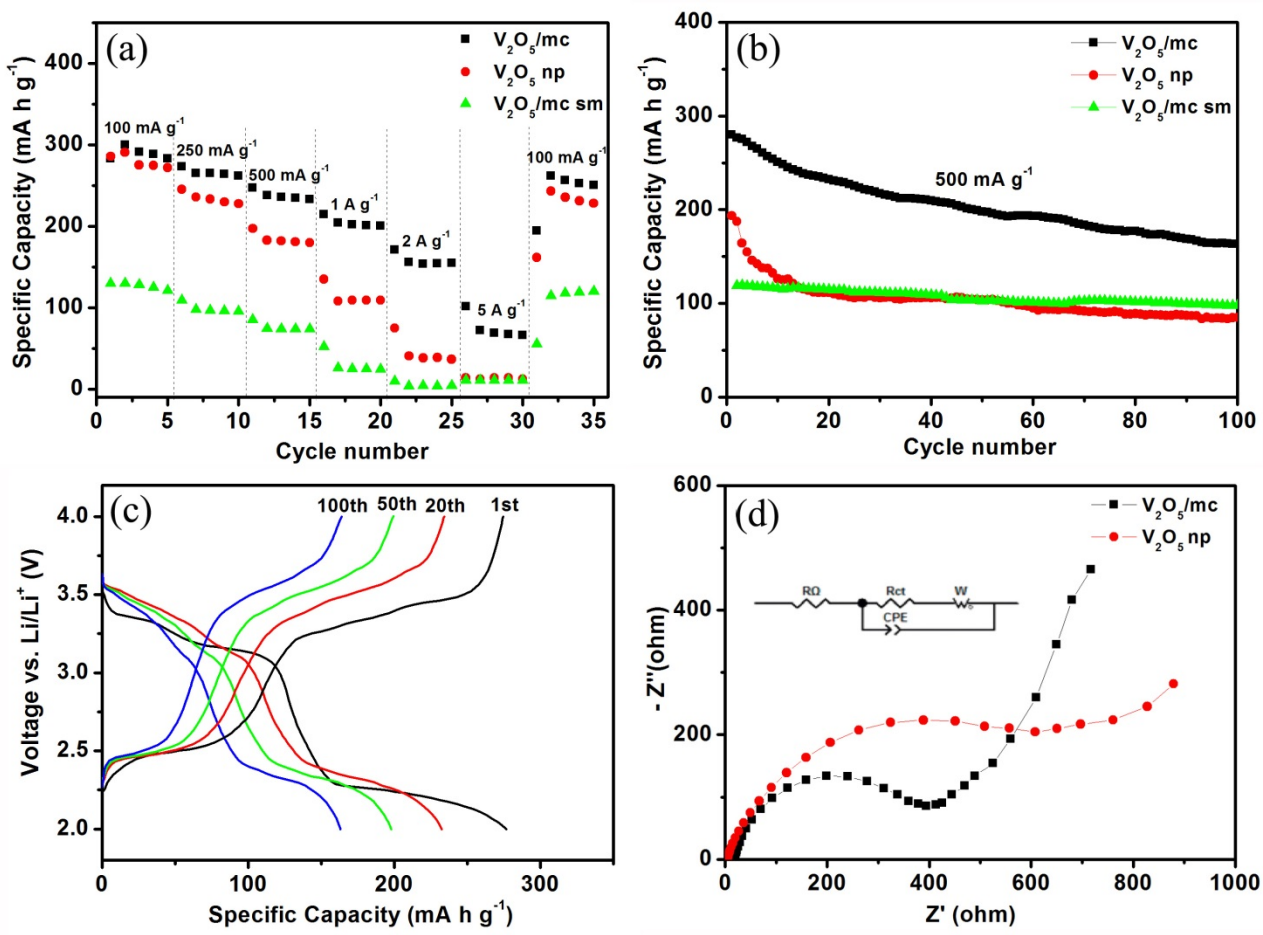

Figure 4. (a) Rate capability of V_2O_5/mc, V_2O_5 n, and V_2O_5/mc sm at various current densities; (b) cycling performance of V_2O_5/mc, V_2O_5 np, and V_2O_5/mc sm in the voltage range of 2.0−4.0 V at the current density of 500 mA g^{-1}; (c) charge/discharge voltage profiles of V_2O_5/mc at the current density of 100 m g^{-1} for the selected cycles indicated; (d) electrochemical impedance spectra of V_2O_5/mc and V_2O_5 np electrodes after 5 charge/discharge cycles and the equivalent circuit used to fit the impedance data (inset).

Table 2. Comparison of our and recently published works on V_2O_5/Carbon composites for lithium ion batteries.

Electrode Description	Rate Capability	Specific Capacity after 50 cycles	Reference
V_2O_5/rGO	220 mAh g^{-1} at 190 mA g^{-1} 180 mAh g^{-1} at 950 mA g^{-1}	105 mAh g^{-1} at 5700 mA g^{-1}	[40]
V_2O_5/PEDOT & MnO_2 nanowire	164 mAh g^{-1} at 100 mA g^{-1} 48 mAh g^{-1} at 500 mA g^{-1}	166 mAh g^{-1}after 40 cycles at 50 mA g^{-1}	[41]
Multiwalled CNT-V_2O_5	250 mAh g^{-1} at 200 mA g^{-1} 221 mAh g^{-1} at 400 mA g^{-1} 193 mAh g^{-1} at 600 mA g^{-1}	199 mAh g^{-1} at 100 mA g^{-1}	[39]
V_2O_5 nanosheet /RGO	200 mAh g^{-1} at 600 mA g^{-1} 138 mAh g^{-1} at 3000 mA g^{-1}	150 mAh g^{-1} at 600 mA g^{-1}	[42]
Graphene nanoribbon/ V_2O_5	200 mAh g^{-1} at 300 mA g^{-1} 165 mAh g^{-1} at 600 mA g^{-1}	230 mAhg^{-1} at 30 mA g^{-1}	[43]
This work	**291 mAh g^{-1}** at **100 mA g^{-1}** **265 mAh g^{-1}** at **250 mA g^{-1}** **247 mAh g^{-1}** at **500 mA g^{-1}**	**198 mAh g^{-1}** at **500 mA g^{-1}**	

Figure 4(c) presents charge/discharge profiles of V_2O_5/mc at a current density of 500 mA g^{-1} in the voltage window of 2.0−4.0 V. There are three plateaus at about 3.3, 3.1, and 2.2 V in the first cycle, which can be attributed to the phase transitions during Li^+ ion intercalation from α-$Li_xV_2O_5$ (x< 0.01) to ε-$Li_xV_2O_5$ (0.35 < x < 0.7), from ε-$Li_xV_2O_5$ to δ-$Li_xV_2O_5$ (x < 1), and from δ-$Li_xV_2O_5$ to γ-$Li_xV_2O_5$ (x > 1), respectively [39]. Three plateaus corresponding to the Li^+ ion deintercalation processes are also occurred on the charge curve. Figure 4(d) shows the Nyquist plots of V_2O_5/mc and V_2O_5 np after five cycles. In the equivalent circuit (inset), R_Ω and R_{ct} reflect the ohmic resistance and the charge transfer resistance, respectively. CPE is the constant phase-angle element, involving double layer capacitance; and W is the Warburg impedance, representing the solid-state diffusion of Li^+ ions into the bulk of the active material. The charge transfer resistance, R_{ct}, for V_2O_5/mc (397 Ω cm^{-2}) is less than that for V_2O_5-np (604 Ω cm^{-2}), indicating

improved charge transfer in the V_2O_5/mc electrode. The reason for the better performance of V_2O_5/mc is likely to be because the V_2O_5 is in a composite with mesoporous carbon, which can provide fast transport channels for lithium ions.

4. Conclusions

We have successfully fabricated a V_2O_5/mesoporous carbon composite by using an ultrasound assisted method followed by sintering. The mesoporous structure of the carbon facilitates the electrolyte diffusion into the bulk of the electrode material and hence provides fast transport channels for Li^+ ions. As a cathode material for LIBs, V_2O_5/mesoporous carbon shows better performance than V_2O_5 nanoparticles, suggesting that V_2O_5/mesoporous carbon composite could be used as a promising cathode material for lithium ion batteries.

Acknowledgements

Mohammad Ihsan is grateful for an Australian Development Scholarship from the Australian Government and for financial support from the Australian Research Council (ARC) through the ARC Centre of Excellence for Electromaterials Science. The authors acknowledge use of facilities within the UOW Electron Microscopy Centre and the Wollongong Isotope Geochronology Laboratory and also thank to Gilberto Cassilas for helping with JEOL ARM-200F (ARC-LE120100104). The authors also thank Dr. Tania Silver for critical reading of the manuscript.

REFERENCES

[1] M. Armand, J.M. Tarascon, Building better batteries, Nature, 451 (2008) 652-657.
[2] J.M. Tarascon, M. Armand, Issues and challenges facing rechargeable lithium batteries, Nature, 414 (2001) 359-367.
[3] J.B. Goodenough, Y. Kim, Challenges for rechargeable Li batteries, Chem. Mater., 22 (2010) 587-603.

[4] Frost & Sullivan, Global lithium-ion market to double despite recent issues, PR Newswire U6, PR Newswire Association LLC, New York, 2013.
[5] T. Ohzuku, Y. Makimura, Layered lithium insertion material of $LiCo_{1/3}Ni_{1/3}Mn_{1/3}O_2$ for lithium-ion batteries, Chem. Lett., (2001) 642-643.
[6] T. Ohzuku, M. Kitagawa, T. Hirai, Electrochemistry of manganese dioxide in lithium nonaqueous cell: I . x-ray diffractional study on the reduction of electrolytic manganese dioxide, J. Electrochem. Soc., 136 (1989) 3169-3174.
[7] A.K. Padhi, K.S. Nanjundaswamy, J.B. Goodenough, Phospho-olivines as positive-electrode materials for rechargeable lithium batteries, J. Electrochem. Soc., 144 (1997) 1188-1194.
[8] Y. Wang, G.Z. Cao, Developments in nanostructured cathode materials for high-performance lithium-ion batteries, Adv. Mater., 20 (2008) 2251-2269.
[9] Y. Wang, K. Takahashi, K. Lee, G.Z. Cao, Nanostructured vanadium oxide electrodes for enhanced lithium-ion intercalation, Adv. Funct. Mater., 16 (2006) 1133-1144.
[10] K.H. Seng, J. Liu, Z.P. Guo, Z.X. Chen, D. Jia, H.K. Liu, Free-standing V_2O_5 electrode for flexible lithium ion batteries, Electrochem. Commun., 13 (2011) 383-386.
[11] A.-M. Cao, J.-S. Hu, H.-P. Liang, L.-J. Wan, Self-assembled vanadium pentoxide (V_2O_5) hollow microspheres from nanorods and their application in lithium-ion batteries, Angew. Chem. Int. Ed., 44 (2005) 4391-4395.
[12] Y.-S. Hu, X. Liu, J.-O. Müller, R. Schlögl, J. Maier, D.S. Su, Synthesis and electrode performance of nanostructured V_2O_5 by using a carbon tube-in-tube as a nanoreactor and an efficient mixed-conducting network, Angew. Chem. Int. Ed., 48 (2009) 210-214.
[13] A.Q. Pan, J.G. Zhang, Z.M. Nie, G.Z. Cao, B.W. Arey, G.S. Li, S.Q. Liang, J. Liu, Facile synthesized nanorod structured vanadium pentoxide for high-rate lithium batteries, J. Mater. Chem., 20 (2010) 9193-9199.
[14] J. Liu, H. Xia, D. Xue, L. Lu, Double-shelled nanocapsules of V_2O_5-based composites as high-performance anode and cathode materials for Li ion batteries, J. Am. Chem. Soc., 131 (2009) 12086-12086.
[15] J. Liu, Y. Zhou, J. Wang, Y. Pan, D. Xue, Template-free solvothermal synthesis of yolk-shell V_2O_5 microspheres as cathode materials for Li-ion batteries, Chem. Comm., 47 (2011) 10380-10382.
[16] Y.L. Cheah, V. Aravindan, S. Madhavi, Electrochemical lithium insertion behavior of combustion synthesized V_2O_5 cathodes for lithium-ion batteries, J. Electrochem. Soc., 159 (2012) A273-A280.
[17] A. Odani, V.G. Pol, S.V. Pol, M. Koltypin, A. Gedanken, D. Aurbach, Testing carbon-coated VO_x prepared via reaction under autogenic pressure at elevated temperature as li-insertion materials, Adv. Mater., 18 (2006) 1431-1436.
[18] C.K. Chan, H. Peng, R.D. Twesten, K. Jarausch, X.F. Zhang, Y. Cui, Fast, completely reversible li insertion in vanadium pentoxide nanoribbons, Nano Lett., 7 (2007) 490-495.
[19] N.S. Ergang, J.C. Lytle, K.T. Lee, S.M. Oh, W.H. Smyrl, A. Stein, Photonic crystal structures as a basis for a three-dimensionally interpenetrating electrochemical-cell system, Adv. Mater., 18 (2006) 1750-1753.
[20] H.-g. Wang, D.-l. Ma, Y. Huang, X.-b. Zhang, Electrospun V_2O_5 nanostructures with controllable morphology as high-performance cathode materials for lithium-ion batteries, Chem. Eur. J., 18 (2012) 8987-8993.
[21] P. Liu, S.H. Lee, C.E. Tracy, Y. Yan, J.A. Turner, Preparation and lithium insertion properties of mesoporous vanadium oxide, Adv. Mater., 14 (2002) 27-30.
[22] C.Q. Feng, S.Y. Wang, R. Zeng, Z.P. Guo, K. Konstantinov, H.K. Liu, Synthesis of spherical porous vanadium pentoxide and its electrochemical properties, J. Power Sources, 184 (2008) 485-488.

[23] D.M. Yu, C.G. Chen, S.H. Xie, Y.Y. Liu, K. Park, X.Y. Zhou, Q.F. Zhang, J.Y. Li, G.Z. Cao, Mesoporous vanadium pentoxide nanofibers with significantly enhanced Li-ion storage properties by electrospinning, Energy Environ. Sci., 4 (2011) 858-861.
[24] J.K. Lee, G.P. Kim, I.K. Song, S.H. Baeck, Electrodeposition of mesoporous V_2O_5 with enhanced lithium-ion intercalation property, Electrochem. Commun., 11 (2009) 1571-1574.
[25] M. Sasidharan, N. Gunawardhana, M. Yoshio, K. Nakashima, V_2O_5 hollow nanospheres: a lithium intercalation host with good rate capability and capacity retention, J. Electrochem. Soc., 159 (2012) A618-A621.
[26] H. Zhao, A. Yuan, B. Liu, S. Xing, X. Wu, J. Xu, High cyclic performance of V_2O_5@PPy composite as cathode of recharged lithium batteries, J. App. Electrochem., 42 (2012) 139-144.
[27] X.X. Li, W.Y. Li, H. Ma, J. Chen, Electrochemical lithium intercalation/deintercalation of single-crystalline V_2O_5 nanowires, J. Electrochem. Soc., 154 (2007) A39-A42.
[28] C.J. Patrissi, C.R. Martin, Sol-gel-based template synthesis and Li-insertion rate performance of nanostructured vanadium pentoxide, J. Electrochem. Soc., 146 (1999) 3176-3180.
[29] A.M. Glushenkov, M.F. Hassan, V.I. Stukachev, Z.P. Guo, H.K. Liu, G.G. Kuvshinov, Y. Chen, Growth of V_2O_5 nanorods from ball-milled powders and their performance in cathodes and anodes of lithium-ion batteries, J. Solid State Electrochem., 14 (2010) 1841-1846.
[30] S.H. Ng, S.Y. Chew, J. Wang, D. Wexler, Y. Tournayre, K. Konstantinov, H.K. Liu, Synthesis and electrochemical properties of V_2O_5 nanostructures prepared via a precipitation process for lithium-ion battery cathodes, J. Power Sources, 174 (2007) 1032-1035.
[31] S. Wang, S. Li, Y. Sun, X. Feng, C. Chen, Three-dimensional porous V_2O_5 cathode with ultra high rate capability, Energy Environ. Sci., 4 (2011) 2854-2857.
[32] X.H. Rui, J.X. Zhu, D. Sim, C. Xu, Y. Zeng, H.H. Hng, T.M. Lim, Q.Y. Yan, Reduced graphene oxide supported highly porous V_2O_5 spheres as a high-power cathode material for lithium ion batteries, Nanoscale, 3 (2011) 4752-4758.
[33] S.Q. Wang, Z.D. Lu, D. Wang, C.G. Li, C.H. Chen, Y.D. Yin, Porous monodisperse V_2O_5 microspheres as cathode materials for lithium-ion batteries, J. Mater. Chem, 21 (2011) 6365-6369.
[34] Y. Yang, S.P. Albu, D. Kim, P. Schmuki, Enabling the anodic growth of highly ordered V_2O_5 nanoporous/nanotubular structures, Angew. Chem. Int. Ed., 50 (2011) 9071-9075.
[35] C.R. Sides, C.R. Martin, Nanostructured electrodes and the low-temperature performance of Li-ion batteries, Adv. Mater., 17 (2005) 125-128.
[36] B. Li, Y. Xu, G. Rong, M. Jing, Y. Xie, Vanadium pentoxide nanobelts and nanorolls: from controllable synthesis to investigation of their electrochemical properties and photocatalytic activities, Nanotechnology, 17 (2006) 2560-2566.
[37] X.F. Zhang, K.X. Wang, X. Wei, J.S. Chen, Carbon-coated V_2O_5 nanocrystals as high performance cathode material for lithium ion batteries, Chem. Mater., 23 (2011) 5290-5292.
[38] L. Mai, L. Xu, C. Han, X. Xu, Y. Luo, S. Zhao, Y. Zhao, Electrospun ultralong hierarchical vanadium oxide nanowires with high performance for lithium ion batteries, Nano Lett., 10 (2010) 4750-4755.
[39] X. Zhou, G. Wu, J. Wu, H. Yang, J. Wang, G. Gao, R. Cai, Q. Yan, Multiwalled carbon nanotubes-V_2O_5 integrated composite with nanosized architecture as a cathode material for high performance lithium ion batteries, J. Mater. Chem. A, 1 (2013) 15459-15468.
[40] W. Shi, X. Rui, J. Zhu, Q. Yan, Design of nanostructured hybrid materials based on carbon and metal oxides for Li ion batteries, J. Phys. Chem. C, 116 (2012) 26685-26693.
[41] L. Mai, F. Dong, X. Xu, Y. Luo, Q. An, Y. Zhao, J. Pan, J. Yang, Cucumber-like V_2O_5/poly(3,4-ethylenedioxythiophene) & MnO_2 nanowires with enhanced electrochemical cyclability, Nano Lett., 13 (2013) 740-745.
[42] J. Cheng, B. Wang, H.L. Xin, G. Yang, H. Cai, F. Nie, H. Huang, Self-assembled V_2O_5 nanosheets/reduced graphene oxide hierarchical nanocomposite as a high-performance cathode material for lithium ion batteries, J. Mater. Chem. A, 1 (2013) 10814-10820.

[43] Y. Yang, L. Li, H. Fei, Z. Peng, G. Ruan, J.M. Tour, Graphene nanoribbon/V_2O_5 cathodes in lithium-ion batteries, ACS Appl. Mater. Interfaces, 6 (2014) 9590-9594.
[44] Y. Qian, A. Vu, W. Smyrl, A. Stein, Facile preparation and electrochemical oroperties of V_2O_5-graphene composite films as free-standing cathodes for rechargeable lithium batteries, J. Electrochem. Soc., 159 (2012) A1135-A1140.
[45] Z. Cao, B. Wei, V_2O_5/single-walled carbon nanotube hybrid mesoporous films as cathodes with high-rate capacities for rechargeable lithium ion batteries, Nano Energy, 2 (2013) 481-490.
[46] Y. Wang, F.B. Su, J.Y. Lee, X.S. Zhao, Crystalline carbon hollow spheres, crystalline carbon-SnO_2 hollow spheres, and crystalline SnO_2 hollow spheres: synthesis and performance in reversible Li-ion storage, Chem. Mater., 18 (2006) 1347-1353.
[47] X. Ji, K.T. Lee, L.F. Nazar, A highly ordered nanostructured carbon-sulphur cathode for lithium-sulphur batteries, Nature Mater., 8 (2009) 500-506.
[48] L. Yu, C.X. Zhao, X. Long, W. Chen, Ultrasonic synthesis and electrochemical characterization of V_2O_5/mesoporous carbon composites, Micro. Meso. Mater., 126 (2009) 58-64.
[49] C.F. Xue, B. Tu, D.Y. Zhao, Evaporation-induced coating and self-assembly of ordered mesoporous carbon-silica composite monoliths with macroporous architecture on polyurethane foams, Adv. Funct. Mater., 18 (2008) 3914-3914.
[50] C.J. Fontenot, J.W. Wiench, M. Pruski, G.L. Schrader, Vanadia gel synthesis via peroxovanadate precursors. 1. in situ laser raman and 51V nmr characterization of the gelation process, J. Phys. Chem. B, 104 (2000) 11622-11631.